Check for updates

Received: 14 July 2019 | Revised: 14 July 2019 | Accepted: 17 July 2019

DOI: 10.1111/ijac.13340

ORIGINAL ARTICLE

International Journal of Applied Ceramic TECHNOLOGY

# The improving thick film properties of $Er_2O_3$ doping *fcc*-$ZrO_2$ type solid electrolyte for SOFC applications

**Esra Yildiz**[1] | **Hilal Özdal**[2] | **Sevgi Ata Kepenek**[2] | **Orhan Türkoğlu**[2]

[1]Department of Chemistry, Yozgat Bozok University, Yozgat, Turkey

[2]Materials Science Research Group, Department of Chemistry, Erciyes University, Kayseri, Turkey

**Correspondence**
Esra Yildiz, Department of Chemistry, Yozgat Bozok University, 66900 Yozgat, Turkey.
Email: esra.korkmaz@bozok.edu.tr

Orhan Türkoğlu, Department of Chemistry, Materials Science Research Group, Erciyes University, 38039 Kayseri, Turkey.
Email: turkoglu@erciyes.edu.tr

**Funding information**
Erciyes University Scientific Research Unit, Grant/Award Number: FBA-2013-4300

**Abstract**

In this study, the binary system of $(ZrO_2)_{1-x}(Er_2O_3)_x$ was investigated in the doping range of $x$; $0.02 \leq x \leq 0.12$ by the Pechini method. According to X-ray diffraction (XRD) measurement results, $Er_2O_3$ doping face-centered cubic (*fcc*) $ZrO_2$-based solid solution was stabilized in the doping range of $0.08 \leq x \leq 0.12$ at 1200°C for 12 hours. Thick films of *fcc*-$ZrO_2$ type powders were produced using ethyl cellulose organic binder mixture and spin-coating method. The crystallographic, microstructural, and electrical conductivity properties of the thick films were characterized via XRD, SEM, and a.c. impedance measurements, respectively. 8-ESZ ($(ZrO_2)_{1-x}(Er_2O_3)_x$, $x = 0.08$) thick film electrolyte showed the highest electrical conduction level which is $2.51 \times 10^{-2}$ ohm$^{-1}$ cm$^{-1}$ at 850°C under 150 mL min$^{-1}$ $O_2$ volumetric flow rate. All thick film properties of *fcc*-ESZ materials were optimized and improved experimentally for using as a solid electrolyte component in solid oxide fuel cell (SOFC) systems. A pre-treatment of 8-ESZ and the cathode-supported type electrochemical cell were primarily fabricated. The power density measurements of 40-LNF ($LaNi_{1-x}Fe_xO_3$, $x = 0.4$) Cathode|Cathode Active (50:50 wt % 40-LNF:8-ESZ)| 8-ESZ Electrolyte|Anode Active (60:40 wt % NiO:8-ESZ)|NiO Anode Electrode cell stack suggest that the produced electrolytes had the usefully properties for SOFC applications.

**KEYWORDS**

$Er_2O_3$, oxide ionic electrical conductivity, solid oxide fuel cell, spin coating, thick film, $ZrO_2$

## 1 | INTRODUCTION

The monoclinic crystal symmetry is well known as the room temperature stable phase of zirconium oxide (zirconia, $ZrO_2$). However, the monoclinic phase transforms allotropically to other polymorphs depending on the heating temperature. During the increasing temperature of the monoclinic phase, the tetragonal and cubic polymorphs of $ZrO_2$ appeared at 1200 and 2400°C, respectively.[1,2] When lower valence cations such as $Y^{3+}$, $Yb^{3+}$, $Er^{3+}$, and $Sc^{3+}$ are doped into the $ZrO_2$ matrix, the tetragonal or the cubic phase can be stabilized at lower temperatures.[3–6] Rare earth–doped zirconia materials show high oxide ion conductivity with a high ionic transport number, close to unity, over a wide oxygen partial pressure range at high temperatures.[4–6] For these reasons, zirconia-based solid electrolyte systems are well-known candidates for some technological applications such as oxygen sensors, fuel cells, and catalytic membrane reactors etc.[7]

The maximum ionic conductivity in $ZrO_2$-based systems is observed when the concentration of acceptor-type dopant is close to the minimum necessary to completely stabilize the cubic fluorite-type phase.[8–11] This concentration (so-called low stabilization limit) and the corresponding conductivity depend on the processing history

 © 2019 The American Ceramic Society 

and microstructural features, such as dopant segregation, impurities, kinetically limited phase transitions, and formation of ordered micro domains. Nevertheless, despite minor contradictions still exist in the literature, for most important systems, the doping concentration ranges providing maximum ionic transport are well established. For example, the highest conductivity levels of the $(ZrO_2)_{1-x}(Y_2O_3)_x$ and $(ZrO_2)_{1-x}(Sc_2O_3)_x$ binary systems are observed in the doping ranges of $x = 0.08$-$0.11$ and 0.09-0.11, respectively. Further additions of doping impurity material decrease $O^{2-}$ ionic electrical conductivity, because of the increasing association effect between the oxygen vacancies and dopant cations. This effect is also resulted the forming complex defects in the crystal structure and lower mobility of oxide ions. It is commonly accepted that this tendency increases with the increasing difference between the host and dopant cationic radius.[10,12–15]

Sol-gel combustion process is a promising technique to produce very fine multi-component oxide ceramic powders in a simple and economic way. The Pechini method is known as an alternative for the conventional sol-gel method.[16] The Pechini-type methods exploit the preparation of homogeneous precursors on a molecular level and enable the preparation of multi-component metal oxides with better homogeneity.[17–19] The method is based on the formation of metal citric acid complexes. The subsequent polymerization of free CA and coordinated CA with ethylene glycol (EG) results in the formation of a polymeric resin. The homogeneous polymeric precursor contains exactly the same metal stoichiometry as the desired product. The metal-CA complexes are thermally stable at temperatures around 130°C and could be "frozen" in a polymer network while preserving in the initial stoichiometric ratios of metal ions in the starting solution. The immobilization of metal cations in such a highly branched polymer can prevent, or at least reduce, the cation mobility during heat treatment which preserves a good dispersion of cations in the product.[18]

As a method for manufacturing a thin electrolyte film, a colloidal process is a very simple and cost-effective way that proves to be less restricted by geometric limitations.[20] As a consequence, slurry coating,[20–22] spin coating,[23,24] dip coating,[25] and tape casting[26] methods have been widely used for the productions of thick films or solid oxide fuel cell (SOFC) systems. Slurry spin-coating method[27] is a combination of slurry coating and spin-coating techniques. Homogeneous and stable zirconia slurry is employed by simply mixing zirconia powders with organic additives consisting of ethyl cellulose and terpineol together, instead of the conventional polymeric zirconia sol or zirconia-ethanol suspension. $ZrO_2$ films do not require the strict heating and cooling rates during the productions without creating the drying treatment in air. Therefore, the procedure has been used as an efficient and fast method for related fabrications.[28]

The aim of this study was planned as the characterization, optimization and improving thick film properties of fcc-type $ZrO_2$ solid electrolyte system. $(ZrO_2)_{1-x}(Er_2O_3)_x$ binary system was investigated in the stoichiometric doping range of $0.02 \leq x \leq 0.12$. The modified Pechini type technique was used for the synthesis of single phase of face-centered cubic (*fcc*)-$ZrO_2$ type materials doped with $Er_2O_3$. Thick films of the *fcc*-ESZ (*fcc* type $ZrO_2$ stabilized with $Er_2O_3$) powders were produced using ethyl cellulose-based organic binder system and slurry spin-coating method. The correct experimental circumstances of thick film fabrications were determinated according to the results of pre-treatments and experimental optimizations. The crystallographic, thermal, microstructural, mechanical strength, thickness, and electrical conductivity properties of *fcc*-ESZ films were investigated by X-ray diffraction (XRD), differential thermal analysis/thermal gravimetry (DTA/TG), scanning electron microscopy (SEM) and a.c. impedance measurement systems. According to the experimental and measurement results, the optimal type of *fcc*-ESZ solid electrolyte was established for the applications of SOFC which can operate at intermediate temperatures.

## 2 | EXPERIMENTAL PROCEDURE

### 2.1 | Synthesis and single cell production

In this study, the binary system of $(ZrO_2)_{1-x}(Er_2O_3)_x$ was studied in the stoichiometric range of $x = 0.02$-$0.12$ with the increment $x = 0.02$ doping amount. The powder materials were prepared using the Pechini method. The starting precursors of $ZrCl_4$ and $Er(NO_3)_3.5H_2O$ (all analytical grade) were added to 50 mL of distilled water under continuous stirring. All the above cation's solution and citric acid were mixed at the stoichiometric ratio. The ratio of the total metal cations (Zr + Er) to citric acid was 4:1. At this stage, EG was added in a molar ratio of EG to citric acid of EG/CA = 4:1. The colorless solution was heated on a hot plate while stirring with a magnetic stirrer to obtain a viscous solution at 80°C. Heating and stirring was continued until the solution started solidifying forming a gel-like porous mass and this gel was dried at 120°C for 24 hours in air. Afterward, the gel was heated to burn out the organic residues and calcined at 900°C for 12 hours. The obtained precursor was then finely ground in a mortar and heated at 1100, 1200°C for 12 hours at each heating temperature, respectively. The wet grindings were also applied with the automatic ball mill system (Retsch, PM 100 model) for the heated powder samples at 1200°C.

The coating slurry for spin-coating process was prepared by mixing of the $(ZrO_2)_{1-x}(Er_2O_3)_x$ ($0.08 \leq x \leq 0.12$). ESZ powders and organic binder system were used for coating mixtures. The organic binder system is appropriate amounts of ethyl cellulose (organic binder), α-terpineol (dispersant),

dibutyl phthalate (plasticizer), toluene (solvent), and ethanol (solvent). The coating mixtures were prepared firstly in a magnetic stirrer for 1 hours, then re-grounded and homogenized in a Jar-Mill with agate balls for 12 hours. Afterward, this slurry was re-mixed in a magnetic stirrer to formation of the viscous coating mixture. Finally, slurry was injected and coated on a surface of tempered glass substrate (25 mm × 25 mm) to form a homogeneous coated layer at spinning speed 1120 rpm of coating system, with ~1 mL injection volumes. All of the coatings were experimented with SCS Cookson type G3-P8 Multi Dispense model spin coater system. These coatings were repeated 10-13 times to produce the ESZ ($(ZrO_2)_{1-x}(Er_2O_3)_x$ ($0.08 \leq x \leq 0.12$)) thick films. As seen in Figure 1, thick layers of ESZ electrolytes (after sintering at 1400°C), which have high density, mechanical strength (non breakable), and uniform were obtained with the outer dimensions of 18 × 18 mm.

In this section, a pre-treatment of 8-ESZ was made for observation of having usable or not available properties of produced electrolyte system for fuel cell applications. For this purpose, a cathode supported, planer-shaped, equipped with five component type electrochemical cell which is signified as "Cathode (LNF)|Cathode Active(LNF + 8-ESZ)|Solid Electrolyte (8-ESZ)|Anode Active (8-ESZ + NiO)|Anode (NiO + Active C)." was used. The single cell was fabricated and measured cell performance and compared with the literature data.

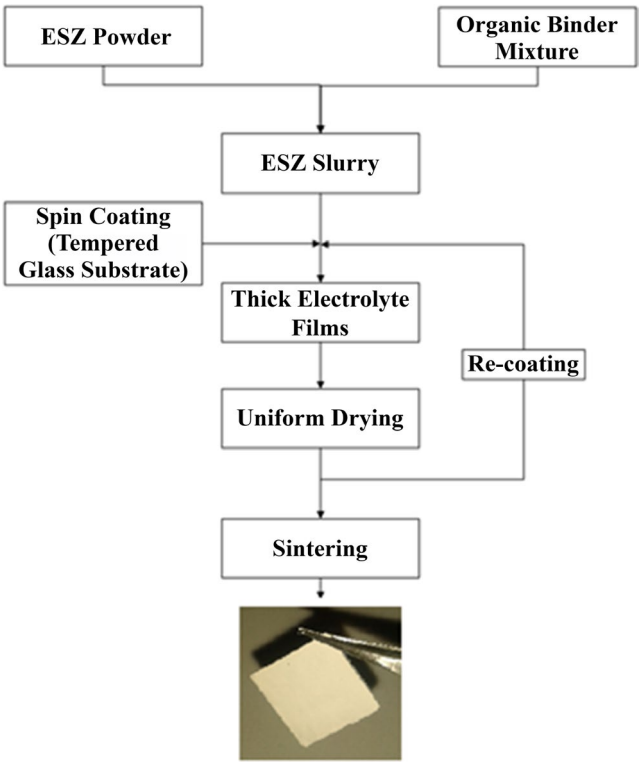



**FIGURE 1** Experimental flowchart for the solid electrolyte thick film production process [Color figure can be viewed at wileyonlinelibrary.com]

## 2.2 | Structure analysis

The XRD data of powders and thick films were recorded using Bruker AXS D8 Advanced diffractometer with a CuKα line of 1.5406 Å. The Win-Index Professional Powder Indexing packet program was used for the indexing of the diffraction peaks in the powder patterns of the samples. The thermal behaviors of the materials were investigated by DTA/TG combined system (Perkin Elmer Diamond). The specimens, usually ~11.5 mg in mass, were heated in the temperature range of 50-1200°C under inert $N_2$ atmosphere with the heating rate of 10°C/min. Measurements were made in dynamic atmosphere using a platinum sample holder and $\alpha$-$Al_2O_3$ inert reference substance. The morphological and microstructural properties were characterized with a LEO 440 model SEM using an accelerating voltage of 20 kV. SEM measurement data were taken from free outer surfaces and cross-sectional surfaces of the thick films.

## 2.3 | Electrical properties

The electrical properties of the thick films were determined by two-probe a.c. impedance measurements. The impedance measurements were carried out by Gamry Interface1000 frequency response analyzer with the Gamry Framework software over the frequency range 1-$10^6$ Hz with an applied potential of 5 mV and 50 data obtained for every temperatures. The conductivity measurements were performed from 400 to 850°C. During measurements the sample temperature was determined by an external thermocouple which was located 5 mm away from the sample. Ag wire (0.25 mm dia, 99.95% purity, Johnson Matthey) and Ag folio (0.025 mm thickness, 99.9% purity, Johnson Matthey) were used for current collectors which were contacted on two outer surfaces of the thick films. The ionic conductivities were calculated using resistance and geometry of samples. Moreover, resistances were determinated from real axis of the Nyquistic impedance plots.

## 2.4 | Power density measurements

The power density of the fabricated fuel cell was measured at ~350-850°C 50°C increments. Humidified $H_2$ was used as the fuel gas and supplied to the anode electrode chamber, whereas the oxidant gas of $O_2$ moved to the cathode electrode surface. After experimental treatments, the most suitable flow rates of $H_2$ and $O_2$ were determined and established at 80 and 160 mL $min^{-1}$, respectively. These flow rates were fixed using with computer controlled flow meters which are Alicat model MC-500 SCCM-D and MC-1 SLPM-D for $H_2$ and $O_2$ correspondingly. In the performance tests, steel-310 type gas serpentine systems were used for providing gases into the cathode

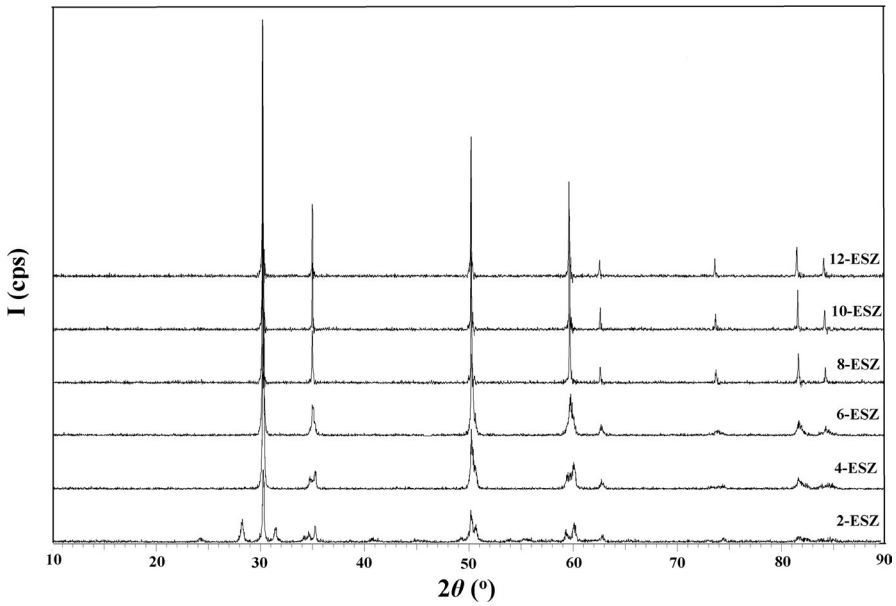



**FIGURE 2** XRD patterns of *fcc*-ESZ powder samples with different $Er_2O_3$ doping concentration (after heating at 1200°C for 12 h)

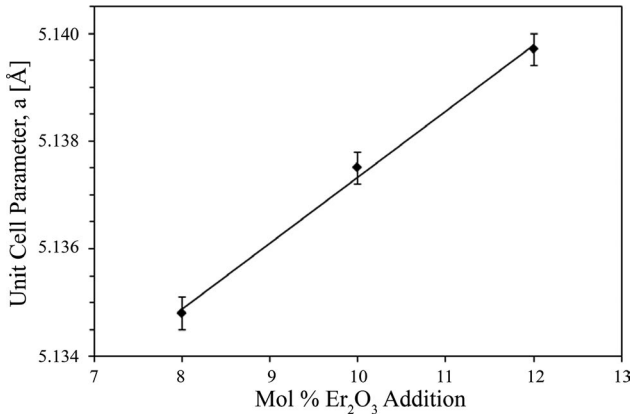



**FIGURE 3** Unit cell parameter variation of *fcc*-ESZ type materials with the doping amount of $Er_2O_3$

and anode electrodes. Thermiculite 866 type (thickness: 1 mm) flexible, compressible, and high temperature stable sheets were used as gas sealing gaskets for the cathode and anode gas serpentine chambers. The frame-shaped gaskets were prepared with the outside and inside dimensions of 2 cm × 2 cm and 1 cm × 1 cm, respectively. Two of them and Ag current collector (99.9% purity, thickness: 0.025 mm) were placed to frame of gas serpentine system with order of sealing, current collector and cathode electrode surface. A same design was applied for the anode half-cell and then mounted single fuel cell test system was compressed with two gas serpentines until preventing of unwanted gas diffusions.

## 3 | RESULT AND DISCUSSION

Figure 2 shows the measured XRD powder patterns of 2-12 mol % $Er_2O_3$ doping $ZrO_2$ which were sintered at 1200°C for 12 hours in air. XRD results showed that material of 2 mol % $Er_2O_3$ doping had multiphase character which contains tetragonal phase predominantly and small amount of monoclinic phase. 4,6-ESZ ceramic samples had single phase property which is in the single tetragonal crystal symmetry. Formation of the *fcc*-$ZrO_2$ type solid solution was observed in the stoichiometric range of 8 and 12 mol % $Er_2O_3$ additions. In this doping range, all of the XRD peaks were indexed in a single face-centered cubic crystal system and their lattice constants were calculated.

The relationship between calculated unit cell parameters of *fcc*-ESZ type materials and doping concentration of $Er_2O_3$ are seen in Figure 3. It was pronounced from the XRD data that erbium ions have been included in the crystal lattice of $ZrO_2$. As shown in this figure, the lattice constants slightly increasing with increasing $Er_2O_3$ content. This lattice parameter variation is in well agreement with effective ionic radii evaluations. The $Zr^{4+}$ cation has smaller ionic radii than $Er^{3+}$ cations (six-coordinated ionic radius are $O^{2-}$:1.40 Å, $Zr^{4+}$: 0.84 Å, $Er^{3+}$: 0.89 Å).[28,29] Accordingly, as the contribution of $Er_2O_3$ increases within $ZrO_2$, the settlement of $Er^{3+}$ cations with higher ionic radii within crystal lattice points causes a regular increase in unit cell constants. The fact that XRD powder patterns have a single unit cell type and slight increasing at unit cell constants indicated that *fcc* phase was appeared as a stable phase and *fcc*-$ZrO_2$ type solid solution formed in higher additive concentrations. Moreover, heating temperatures of below 1200°C were determinated as insufficient reaction temperatures, because all the studied samples ($0.02 \leq x \leq 0.12$) had a heterogeneous character according to their XRD measurements. Therefore, 1200°C was observed as the minimum reaction temperature for the formation of the single phase materials. It was planned that

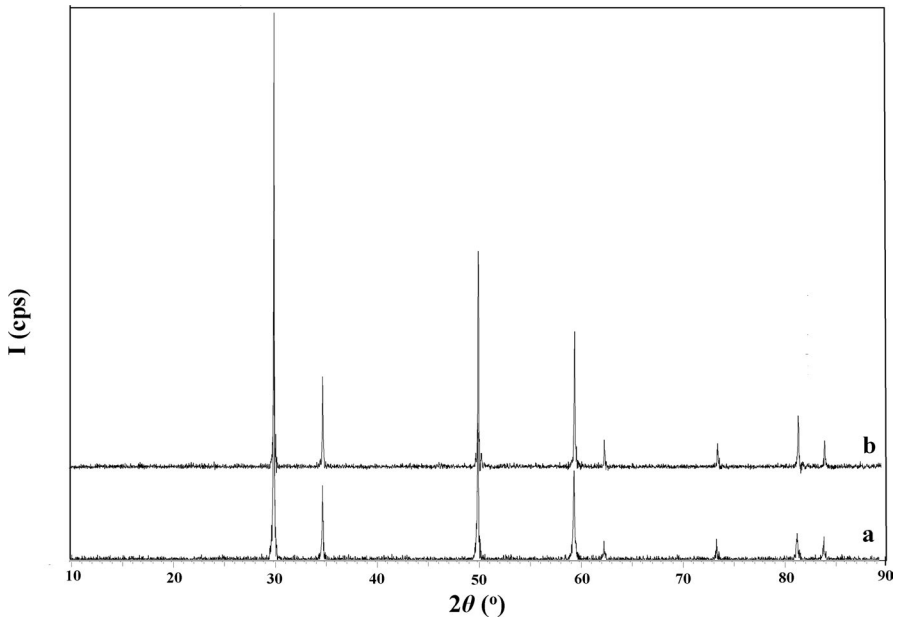



**FIGURE 4** XRD patterns of 8-ESZ sample: (A) thick film (after heating at 1400°C, for 18 h), (B) powder (after heating at 1200°C, for 12 h)

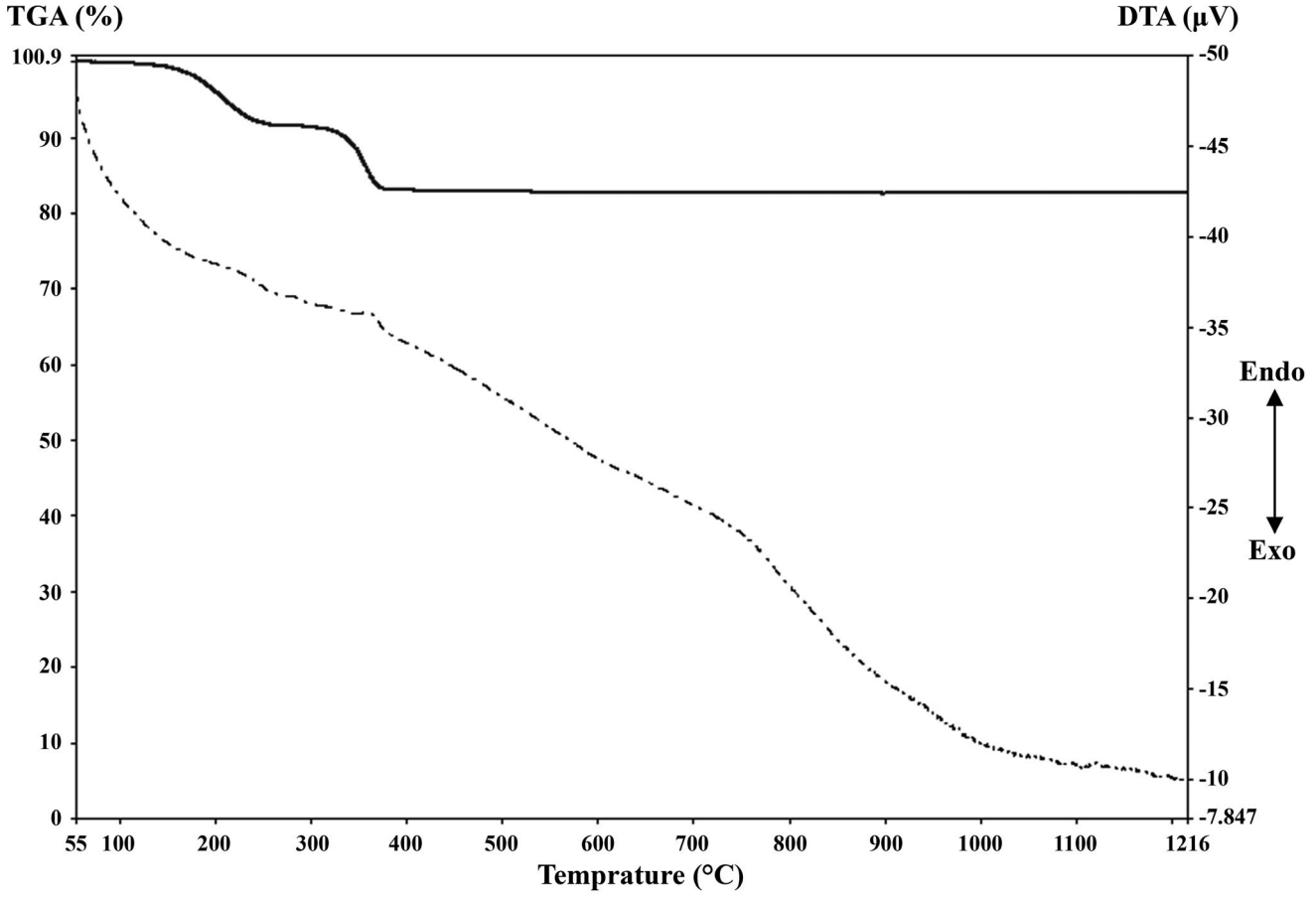



**FIGURE 5** DTA/TG diagrams of 8-ESZ thick film

production thick films of *fcc* type powder materials in the doping range of $0.08 \leq x \leq 0.12$. The production and investigation thick film of tetragonal and related multiphase powder materials were not included in this study. Effect of the thick film production process on phase stabilization of *fcc*-ESZ was also investigated by XRD measurements. Figure 4 shows XRD spectrums of 8-ESZ powder and its thick film. As seen in Figure 4, all diffraction peaks of

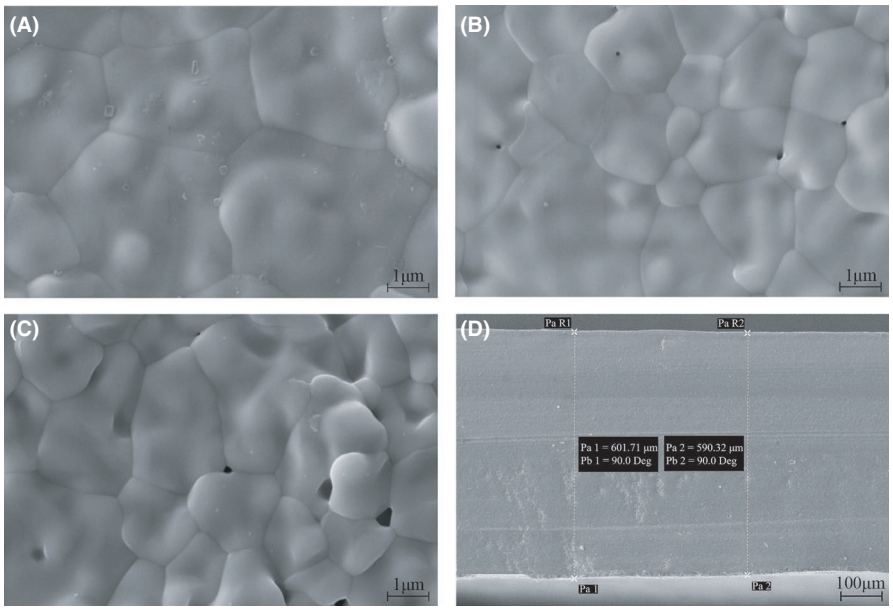



**FIGURE 6** Measured free outer and fracture surfaces SEM images of *fcc*-ESZ thick films: (A) 8-ESZ, (B) 10-ESZ, (C) 12-ESZ, (D) 8-ESZ (cross-sectional surface)

powder and film samples overlap, and no difference between patterns was observed. This observation indicated that the coating, sintering experiment and thick film process do not cause a decomposition effect or formation of unwanted chemical reactions on the *fcc*-ESZ type thick layers.

The measured DTA/TG diagrams of unheated 8-ESZ crude coating film are seen in Figure 5. On the TG curve, a considerable mass lose (~20 wt %) was observed at the temperature range of 100-400°C. In this temperature range, any endothermic effect was not observed. Therefore, this observed weight loss was characterized as a volatilization of organic binder system without melting. Alternatively, any exothermic or endothermic peak was not detected on the DTA graph up to 1250°C. This result indicated that the formed 8-ESZ thick film has not any phase transition and shows a high thermal stability up to around 1250°C. The DTA/TG curves of other *fcc*-thick films observed were quite similar to the curves given in this figure.

SEM measurements were performed to *fcc*-ESZ type thick films for microstructure evaluation, particle size determination, densification, porosity, and thickness. The measured SEM images are seen in Figure 6. SEM outer surface micrographs of 8,10,12-ESZ films indicated that particle size distributions are not uniform and homogeneity of particle distributions reduce with increasing the doping amount of $Er_2O_3$. The particle sizes were observed around 4 μm for 8-ESZ sheet which has highest uniformity of particle distribution and smoothest surface, whereas 10,12-ESZ thick films have 1-2 μm. This observation showed that particle size decreases with increasing mol % $Er_2O_3$ addition. 10,12-ESZ materials have even higher number of grains, insufficient smooth of particles, weaker densification and less homogeneity of particle distributions. In addition, porosities increase with increasing the doping content of $Er_2O_3$. These results showed that decreasing of the doping concentration cause to appearing of better microstructural aspects which are observed for 8-ESZ sheet. Since electrical conductivity properties of *fcc*-$ZrO_2$ type materials mostly depends on their microstructural aspects. It is expected that samples with higher porosity, greater number of grains and lower densification may cause to observation on lower levels of the electrical conductions. An example fracture surface SEM image of 8-ESZ is shown in Figure 6D. It was comprehended that this range is sufficient for performing characterizations. The thickness of sheet was determinated as 350-400 μm (after sintering at 1400°C) for 10-13 times of repeated coating process. Also, porosity was observed as a negligible level which can be correlated with highest mechanical strength of 8-ESZ layer. Additionally, fracture surface SEM image which was taken from four different points of the sheet resulted in an insignificant difference between measurements. This implied to use of a good and homogeneous coating process during the productions of thick films.

The measured electrical conductivity plots of $\log\sigma - (10^3/T)$ for 8, 10, 12-ESZ films are presented in Figure 7. The conductivities were calculated from experimental data using the equation of $\sigma = (1/R)(t/A)$. Where $\sigma$ is the thick film electrical conductivity, $t$ (cm) is thickness of *fcc*-ESZ film, $A$ ($cm^2$) is active surface area of layer surrounded with Ag current collector, and $R$ (ohm) is observed resistance of sheet which is determinated from the measured impedance plots. The impedances were founded from interceptions of the observed semicircle on real axis of the impedance spectra. These data were obtained during repeated heating runs at a constant heating rate in air.

As seen in Figure 7, the conductivities of thick films increase sharply with the increasing temperature between 400

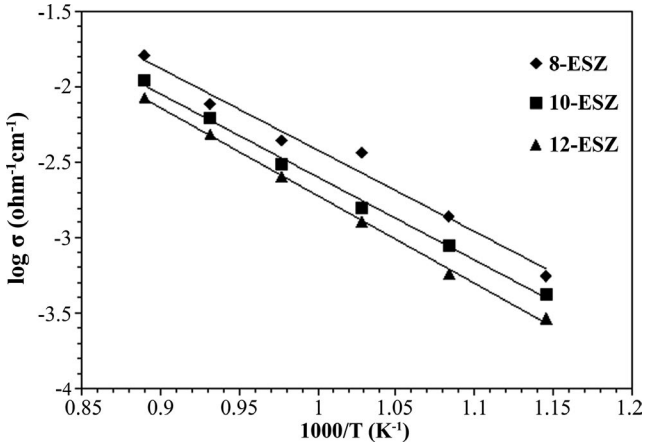



**FIGURE 7** Temperature dependence electrical conductivity of *fcc*-ESZ thick films in air atmosphere

and 850°C. The highest electrical conductivity was observed as $1.62 \times 10^{-2}$ ohm$^{-1}$ cm$^{-1}$ for 8-ESZ solid electrolyte at 850°C. Because of log vs (1/*T*) exhibits a linear relationship at temperature range between 400 and 850°C, we decided that this behavior of the conductivity can be described by Arrhenius equation; $\sigma = \sigma_o \exp(-Ea/kT)$. In the formula; $\sigma$, $\sigma_o$, *Ea*, k, and *T* are observed electrical conductions of thick films, pre-exponential factor, activation energy for the mobile oxygen ions (proportional to the slope), Boltzmann constant, and absolute temperature, respectively.

$ZrO_2$-based solid electrolyte systems are well known as the oxide ionic type electrical conductors and their lattice defect formations reaction can be defined by Kroger and Vink notation[29–31]:

$$Er_2O_3 \rightarrow 2Er'_{Zr} + V_{\ddot{O}} + 3O^x_O$$

where; $2Er'_{Zr}$ represent $Er^{3+}$ occupying lattice sites which are occupied normally by $Zr^{4+}$ cations, $V_{\ddot{O}}$ denote the oxide anionic vacancies, and $O^x_O$ is the oxygen atom, respectively. This theoretical approximation indicated that the lattice point substations between Zr and Er cations occur in *fcc* crystal structure during the formed reaction of $ZrO_2$ with $Er_2O_3$ doping. Because of the charge balance, these cationic substations cause the formation of oxygen anionic vacancies in the crystal lattice. These anionic defects result in showing an oxide ionic type electrical conductivity of the produced *fcc*-$ZrO_2$ thick films. Therefore, possible reason of increasing the conductivities with increasing temperature was proposed since the increasing mobility of the interstitial $O^{2-}$ ions with the temperature. At elevated temperatures, thermal vibration energy of ions increases causing higher oxygen ionic movement rate along with the interstitial tetrahedral lattice points. Additionally, the theoretical of oxide anionic conductivity can be defined simply as follows[32,33]:

$$\sigma_{\text{ionic}} = 2n\,|e|\,\mu$$

In the equation; *n*, e, and $\mu$ are the carrier density, elementary electric charge, and mobility of oxide ion, respectively. The number of charge carries and the mobility makes an increment effect for electrical conduction. Although interstitial $O^{2-}$ vacancies are present in crystal lattice, thermal energy of some charge carrier anions is not enough for jumping to the nearest neighbor tetrahedral vacancy points at low temperatures. In other words, lower mobility of carrier cause to decay the movement of oxygen ions, then reducing the level of the electrical conductivity. Therefore, thick layer materials show a lower electrical conductivity level (~$10^{-4}$ ohm$^{-1}$ cm$^{-1}$) at lower temperatures. At high temperatures, thermal vibrations of carries may also assist jumping process momentarily by either shortening jumping distances or by widening jumping conduction pathways through the crystal lattice. Also, it can be expected that the disordered arrangement of oxide ions and $O^{2-}$ vacancies may dominantly appear at higher temperatures than their ordered locations at lower temperatures. This disorder structure can also play an important role for exhibiting of higher mobility, easier movement of carriers, and the increment result of the electrical conduction.

Figure 8 shows the conductivity isotherms of *fcc*-ESZ samples depending on the mol % $Er_2O_3$ addition in air. The electrical conductivity of $Er_2O_3$ doped *fcc* type solid solution decreases systematically with the increasing of $Er^{3+}$ substitution with host Zr ions and 8-ESZ has a maximum degree of electrical conductivity. For this material, the observed values were $4.47 \times 10^{-3}$ and $1.62 \times 10^{-2}$ ohm$^{-1}$ cm$^{-1}$ at 750 and 850°C, respectively. Materials of 10 and 12-ESZ showed lower electrical conductivity level than 8-ESZ thick film. At 850°C, their conductivities were observed as $1.10 \times 10^{-2}$ and $8.51 \times 10^{-3}$ ohm$^{-1}$ cm$^{-1}$ for 10 and 12-ESZ, respectively. The observed level of the conductivities at 850°C showed that 8,10,12-ESZ systems had a solid electrolyte character which can be used as an important component for producing solid oxide fuel cells. Usually, the high electrical conductivity level of the solid electrolyte can cause the increasing of electrochemical energy production performance of the SOFC systems.

In the theory, it is well-known phenomenon that electrical conductivity should increase with the increasing $O^{2-}$ vacancy concentration in the most oxide ionic conductors. However, the number of $O^{2-}$ vacancies is not just one factor for the level of the observed conductivities. In addition to this effect, many other factors which are crystallographic and microstructure properties also play important roles on the degree of the electrical conductivities. The observation of decreasing electrical conductivity with the increasing doping of mol % $Er_2O_3$ additions was in agreement with the microstructure

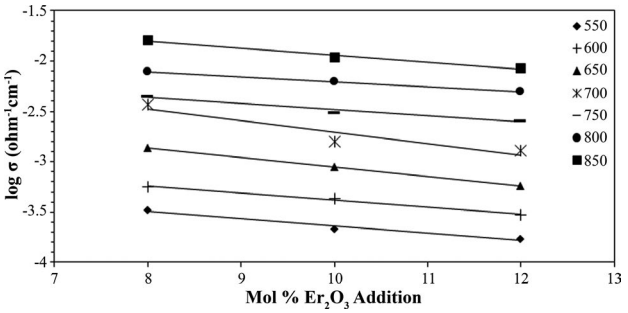



**FIGURE 8** $Er_2O_3$ doping concentration dependence electrical conductivities at different temperatures and in air atmosphere

properties of *fcc*-ESZ ceramic electrolytes. With increasing $O^{2-}$ vacancies, the observed electrical conductivities decrease with increasing $Er_2O_3$ content. This result showed that the observed grain sizes, porosities, surface flatness, and densifications of the thick films became dominant effects more than their increasing effect of oxide ionic vacancies. Therefore, the predominant effects resulted in reducing the level of electrical conductivity with the increasing of doping concentration. Because, microstructure and $O^{2-}$ ionic transport relationships are well known effects for oxide ionic conductivity of the ceramic electrolytes. This phenomenon is called as the grain-boundary effect which leads to a reduction of several order magnitudes of the electrical conductivity. In fact, high porosity and low connectivity between grains have a decreasing effect in the transport processes. Generally, the grain-boundary conductivity ($\sigma_{gb}$), which decreases with increasing number of grains, has an important role for the oxygen ionic transport mechanism for the ceramic electrolyte materials. As shown in Figure 6, grain sizes vary with the amount of $Er_2O_3$ addition. The number of grain boundaries and porosity increase consistently whereas densification, particle size, connectivity of grains, surface flatness, and homogeneity of particle distributions decrease with the increasing of the doping concentration of $Er_2O_3$. These observations were in agreement with the fact that the SEM picture of 10 and 12-ESZ systems which have lower oxygen ionic conductivity. These thick films have high number of grain boundaries, weaker surface smoothness, and high degree of porosity. These observed microstructural properties form "insulating barriers" or "blocking effects" for the grain-boundary conductivity and transport of oxide ions. Therefore, both $\sigma_{gb}$ and $\sigma_{Thick\ film}$ decrease with the doping concentration of $Er_2O_3$.

The measured electrical conductions of ESZ thick film electrolytes which are under 150 mL $min^{-1}$ flow rate of $O_2$ are presented in Figure 9. As seen in Figure 9, the temperature dependence of electrical conductivity variations in oxygen atmosphere is nearly similar with their air atmosphere conductivities correspondingly. The electrolyte material of 8-ESZ has the highest conductivity. The regular increasing of oxygen atmosphere electrical conduction with temperature showed that the produced solid electrolytes have Arrhenius type electrical conductivity behavior. However, it was also determined that oxygen atmosphere electrical conductions was nearly two times higher than their air atmosphere conductivities. Oxygen atmosphere causes to increase the number of $O^{2-}$ charge carries more than their air atmosphere and makes an increasing effect for conductions.

Figure 10 shows the effect of $O_2$ flow rate on the level of 8-ESZ electrical conductivity. At low temperatures (~600, 650°C), electrolyte system has a low electrical conductivity level and the increasing of oxygen flow rate do not cause a noticeable difference on the degree of conductions. This result was connected with insufficient thermal activation energy of $O^{2-}$ ions. As discussed earlier, $O^{2-}$ ions can not move to nearest neighbor $O^{2-}$ vacancy lattice points at low temperatures and the low level of electrical conductivity may be correlated with the electronic type conductivity which is formed by the weak electron delocalization of $Er^{3+}$ and $Zr^{4+}$ valence electrons. However, the conductivity level of the electrolyte increases systematically with flow rate of $O_2$ at 850°C. Therefore, it was supposed that the studied electrolyte systems show an oxygen anionic type electrical conductivity dominantly at high temperatures (especially above 800°C).

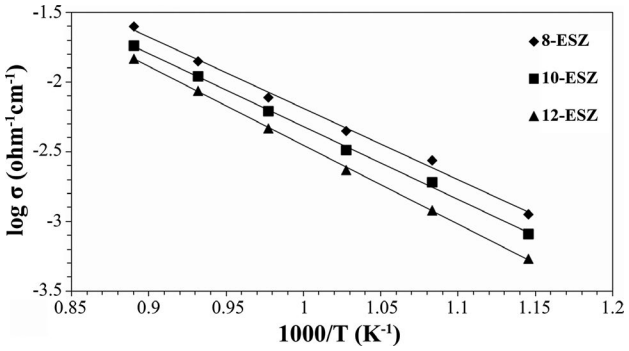



**FIGURE 9** Observed electrical conductivities of *fcc*-ESZ thick films depending on the temperature (under 150 mL $min^{-1}$ flow metric rate of $O_2$ dynamic atmosphere)

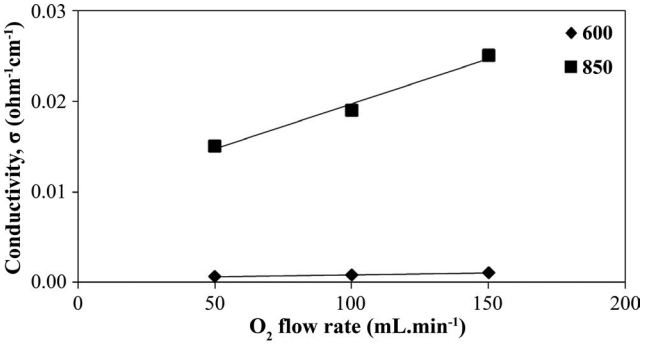



**FIGURE 10** Measured electrical conductivity of 8-ESZ solid electrolyte depending on the oxygen gas flow rate at constant temperature 850°C

All of the characterization and experimental optimization results indicated that the produced materials can be used as a solid electrolyte component for the fabrication of SOFC. In this way, we planned a basic and pre-treatment SOFC application of 8-ESZ electrolyte which has highest electrical conductivity in air and $O_2$ atmospheres. It was aimed from these pre-applications for determination the availability of 8-ESZ material which can be used as a solid electrolyte component in SOFC system. The detail investigations and productions of the *fcc*-ESZ type SOFC systems were left out scope of this presented study. The fracture surface SEM image of cathode supported with five components and 8-ESZ type electrochemical cell is seen in Figure 11. The SEM micrograph showed good connectivity between layers of SOFC components which are the cathode, cathode active, 8-ESZ electrolyte, anode active and anode, respectively. It was also observed that the produced cell stack had a high mechanical strength, densification and smooth surfaces. Thicknesses of the layers were observed as around 670.98, 28.33, 59.48 μm for cathode electrode plus cathode active, 8-ESZ electrolyte and anode active plus anode electrode correspondingly. The observed power densities of the electrochemical cell stack which is: "40-LNF Cathode|Cathode Active (50:50 wt % 40-LNF:8-ESZ)|0.8-ESZ Electrolyte|Anode Active (60:40 wt % NiO:8-ESZ)|NiO Anode Electrode" depending on operating temperatures is shown in Figure 12, under $H_2$ and $O_2$ constant volumetric flow rates of 80 and 160 mL $min^{-1}$, respectively. This measurement concluded that highest power density was around 90 $mWcm^{-2}$ at operating temperature of 850°C. According to the comparing of literature data, the observed maximum value of power density was an acceptable level which implied that 8-ESZ electrolyte has the correct crystallographic, microstructural, electrical conductivity, and useful properties for the SOFC production. Although acceptable level of the observed power density, it was also supposed to be an insufficient power density level for the 8-ESZ type SOFC system which needs other improving and optimizations

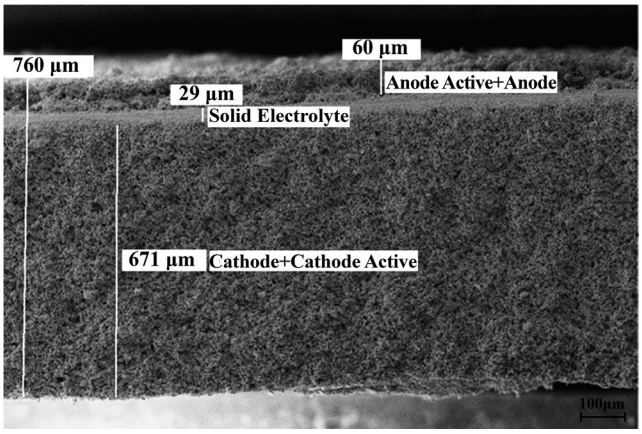



**FIGURE 11** Fracture surface SEM image of cathode supported and 8-ESZ solid electrolyte type SOFC system

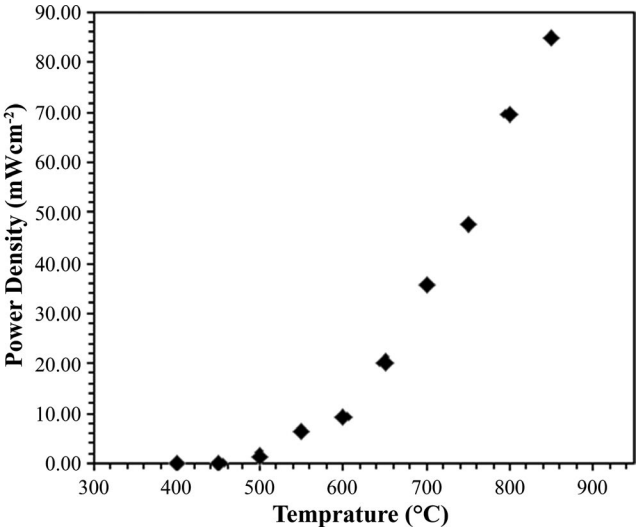



**FIGURE 12** Observed power densities of "40-LNF Cathode|Cathode Active (50:50 wt % 40-LNF:8-ESZ)|0.8-ESZ Electrolyte|Anode Active (60:40 wt % NiO:8-ESZ)|NiO Anode Electrode" single electrochemical cell depending on the temperature (under constant volumetric rates; $H_2$ = 80 mL $min^{-1}$, $O_2$ = 160 mL $min^{-1}$)

for the production of higher electrochemical energy. These SOFC-related major optimizations were considered like the treatments of different type of cathode electrodes, the composition of anode active layer, surveying the thicknesses of all component layers and experimental conditions of single cell stack productions. Therefore, necessary recovering and optimizations were planned as a second part of *fcc*-ESZ type SOFC's investigation by our research group.

## 4 | CONCLUSIONS

$(ZrO_2)_{1-x}$ $(Er_2O_3)_x$ binary system was investigated in stoichiometric $Er_2O_3$ doping range of $x$; $0.02 \leq x \leq 0.12$ by the Pechini method. Single phase of *fcc* type $ZrO_2$-based powder materials were observed $Er_2O_3$ doping range of $0.08 \leq x \leq 0.12$ at 1200°C for 12 hours according to XRD measurement results. $Er_2O_3$ doping amount versus lattice parameters of the *fcc*-ESZ materials were in good agreement with the ionic radius of $Er^{3+}$ and $Zr^{4+}$ cations. The thick films of the 8,10,12-ESZ powder samples were produced by spin-coating method and ethyl cellulose-based mixture was used as an organic binder system which can volatilize at 100-400°C temperature range from the unheated coated sheets according to the DTA/TG results. After experimental treatments and all of the thick film production parameters which are the stoichiometric ratio of organic binder mixture, the amount of *fcc*-ESZ powders, coating periods, spinning speeds of coating, sintering temperature, and period of coated layers were determined. The thick films were obtained after

sintering at 1400°C for 12 hours and their crystallographic, microstructural, and electrical conductivity properties were optimized for SOFC applications. The electrical conductivity measurement results showed that 8,10,12-ESZ thick films had a solid electrolyte character and they had a predominant $O^{2-}$ ionic type electrical conduction at high temperatures. The electrolyte of 8-ESZ film showed highest conductivity which is $2.51 \times 10^{-2}$ ohm$^{-1}$ cm$^{-1}$ at 850°C and under 150 mL min$^{-1}$ $O_2$ volumetric flow rate. Moreover, it had most suitable microstructure properties which are the lowest porosity, the highest grain size, good surface smoothness, higher mechanical strength, and densification. Therefore, the improved and optimized thick film of 8-ESZ was used primarily as a solid electrolyte component in its application of LNF cathode supported electrochemical cell stack. The power density and SEM results of these pre-treatments indicated that the produced *fcc*-ESZ electrolytes have suitable characteristics for different types of SOFC's fabrications.

## ACKNOWLEDGMENTS

This work was financially supported by Erciyes University Scientific Research Unit (EÜBAP, Grant No: FBA-2013-4300).

## ORCID

*Esra Yildiz* https://orcid.org/0000-0002-6481-4658
*Orhan Türkoğlu* https://orcid.org/0000-0002-9703-5554

## REFERENCES

1. Abriata JP, Garces J, Versaci R. The O-Zr (Oxygen-Zirconium) system. Bull Alloy Phase Diagr. 1986;7:116–24.
2. Wang WE, Olander DR. U-O and Zr-O thermochemistry from the pure metal to the dioxide and application to core-concrete interactions in severe fuel damage accident analysis. J Nucl Mater. 1993;201:231–7.
3. Tekeli S, Aktaş B, Küçüktevek M. Microstructural and mechanical properties of $Er_2O_3$-$ZrO_2$ ceramics with different $Er_2O_3$ contents. High Temp Mater Proc. 2012;31:701–6.
4. Minh NQ, Takahashi T. Science and technology of ceramic fuel cells. Amsterdam: Elsevier; 1995: p. 69–70.
5. Ishihar T, Sammes NM, Yamamoto O. Chapter 4: Electrolytes. In: Carter Singhal SC, Kendall K, editors. High temperature solid oxide fuel cells-fundamentals, design and applications. Oxford: Elsevier, 2003; p. 83–8.
6. Yıldız E, Yılmaz S, Türkoğlu O. The production and characterization of ytterbium-stabilized zirconia films for SOFC applications. Int J App Ceram Technol. 2016;13:100–7.
7. Verkerk MJ, Middelhuis BJ, Burggraaf AJ. Effect of grain boundaries on the conductivity of high-purity $ZrO_2$-$Y_2O_3$ ceramics. Solid State Ionics. 1982;6:159–70.
8. Etsell TH, Flengas SN. Electrical properties of solid oxide electrolytes. Chem Rev. 1970;70:339–76.
9. Kharton VV, Naumovich EN, Vecher AA. Research on the electrochemistry of oxygen ion conductors in the former Soviet Union. I. $ZrO_2$-based ceramic materials. J Solid State Electrochem. 1999;3:61–81.
10. Yamamoto O, Arachi Y, Sakai H, Takeda N, Imanishi N, Mizutani Y, et al. Zirconia based oxide ion conductors for solid oxide fuel cells. Solid State Ionics. 1998;52:23–32.
11. Inaba H, Tagawa H. Zirconia-based solid electrolytes: microstructure, stability and ionic Conductivity. Solid State Ionics. 1992;52:23–32.
12. Inaba H, Tagawa H. Ceria-based solid electrolytes. Solid State Ionics. 1996;83:1–16.
13. BouwmeesterHJM, Burggraaf AJ. Chapter 10: Dense ceramic membranes for oxygen separation. In: Carter Cot L, editor. Fundamentals of inorganic membrane science and technology. Amsterdam: Elsevier, 1996; p. 435–40.
14. Sammes NM, Tompsett GA, Nafe H, Aldinger F. Bismuth based oxide electrolytes-structure and ionic conductivity. J Eur Ceram Soc. 1999;19:1801–26.
15. Mogensen M, Sammes NM, Tompsett GA. Physical, chemical and electrochemical properties of pure and doped ceria. Solid State Ionics. 2000;129:63–94.
16. Pechini MP. Method of preparing lead and alkaline-earth titanates and niobates and coating method using the same to form a capacitor. US Patent, 1967;3:330–697.
17. Zhang Y, Yang Y, Tian S, Chunsheng I, Chunhua Y. Sol–gel synthesis and electrical properties of $(ZrO_2)_{0.85}(REO_{1.5})_{0.15}$ (RE = Sc, Y) solid solutions. J Mater Chem. 2002;12:219–24.
18. Gaudon M, Laberty-Robert C, Ansart F, Stevens P, Rousset A. Preparation and characterization of $La_{1-x}Sr_xMnO_{3+\delta}$ ($0 \le x \le 0.6$) powder by sol–gel processing. Solid State Sci. 2002;4:125–33.
19. Kakihana M. Invited review "sol-gel" preparation of high temperature superconducting oxides. J Sol-Gel Sci Technol. 1996;6:7–55.
20. Kim SD, Hyun SH, Moon J, Hee J, Kim JH, Song RH. Fabrication and characterization of anode-supported electrolyte thin films for intermediate temperature solid oxide fuel cells. J Power Sources. 2005;139:67–72.
21. Cai Z, Lan TN, Wang S, Dokiya M. Supported Zr(Sc)$O_2$ SOFCs for reduced temperature prepared by slurry coating and co-firing. Solid State Ionics. 2002;152:583–90.
22. Yoon SP, Han J, Nam SW, Lim T-H, Oh I-H, Hong S-A, et al. Performance of anode-supported solid oxide fuel cell with $La_{0.85}Sr_{0.15}MnO_3$ cathode modified by sol–gel coating technique. J Power Sources. 2002;106:160–6.
23. Kim SG, Yoon SP, Nam SW, Hyuh SH, Hong SA. Fabrication and characterization of a YSZ/YDC composite electrolyte by a sol-gel coating method. J Power Sources. 2002;110:222–8.
24. Xu XY, Xia CR, Huang SG, Peng D. YSZ thin films deposited by spin-coating for IT-SOFCs. Ceram Int. 2005;31:1061–4.
25. Xia CR, Zha SW, Yang WG, Peng R, Meng G. Preparation of yttria stabilized zirconia membranes on porous substrates by a dip-coating process. Solid State Ionics. 2002;133:287–94.
26. Meier LP, Urech L, Gauckler LJ. Tape casting of nanocrystalline ceria gadolinia powder. J Eur Ceram Soc. 2004;24:3753–8.
27. Ai NA, Lü Z, Chen K, Huang X, Wei BO, Zhang Y, et al. Low temperature solid oxide fuel cells based on $Sm_{0.2}Ce_{0.8}O_{1.9}$ films fabricated by slurry spin coating. J Power Sources. 2006;159:637–40.
28. Chen K, Lü Z, Ai NA, Huang X, Zhang Y, Xin X, et al. Development of yttria-stabilized zirconia thin films via slurry spin coating for

intermediate-to-low temperature solid oxide fuel cells. J Power Sources. 2006;160:436–8.
29. Yamamoto O, Arati Y, Takeda Y, Imanish N, Mizutani Y, Kawai M, et al. Electrical conductivity of stabilized zirconia with ytterbia and scandia. Solid State Ionics. 1995;79:137–42.
30. Borowiec MT, Prochorov AA, Prochorov AD, Dyakorov VP, Szymczak H. Electron paramagnetic resonance spectra of $Er^{3+}$ in the monoclinic $KY(WO_4)_2$ crystal. J Phys Condens Matter. 2003;15:5113–7.
31. Carnall WT, Fields PR, Rajnak K. Electronic energy levels in the trivalent lanthanide aqua ions I. Pr3+, Nd3+, Pm3+, Sm3+, Dy3+, Ho3+, Er3+, and Tm3+. J Chem Phys. 1968;49:4424–9.
32. Bozoklu M, Türkoğlu O, Yılmaz S, Arı M. Oxide ionic conductivity and crystallographic properties of tetragonal type $Bi_2O_3$-based solid electrolyte doped with $Ho_2O_3$. Mater Sci Tech. 2010;26:1239–47.
33. West AR. Basic solid state chemistry. 2nd ed. Chichester: John Wiley and Sons; 1998: p. 520–45.

**How to cite this article:** Yildiz E, Özdal H, Kepenek SA, Türkoğlu O. The improving thick film properties of $Er_2O_3$ doping *fcc*-$ZrO_2$ type solid electrolyte for SOFC applications. *Int J Appl Ceram Technol*. 2020;17:1293–1303. https://doi.org/10.1111/ijac.13340